https://doi.org/10.5194/egusphere-2026-3289
Preprint. Discussion started: 2 July 2026

Cloud environment controls the precipitation response to liquid propane (LP) seeding: an ice nucleation parameterization for LP seeding and idealized simulations

Sisi Chen, Lulin Xue, Michelle Harrold, Sarah Tessendorf, Jamie Wolff, Nick Dawson, and Darcy Jacobson

Research Applications Laboratory, NSF National Center for Atmospheric Research, Boulder, Colorado

Correspondence to: Sisi Chen (sisichen@ucar.edu)

Abstract. This study presents a liquid propane (LP) seeding parameterization in the Weather Research and Forecasting (WRF) model. Two formulas derived from laboratory experiments express ice production as a function of temperature and LP release rate. The seeding impacts on clouds and precipitation are evaluated through idealized two-dimensional simulations spanning two mountain heights, four environmental soundings, and four seeding scenarios. The simulations reveal an environment-dependent microphysical response in which the ice conversion process near the seeding site varies with the natural rain efficiency, from a snow-dominated regime where riming is limited to a riming-dominated regime in efficient-rain conditions. The largest enhancement occurs in the low mountain, where supercooled liquid water (SLW) persists and natural precipitation remains weak. Seeding impacts in the high mountain are weaker, with a mild reduction in total precipitation in the case where the natural rain process is most efficient. Snow enhancement dominates the net total precipitation increase. Compared with AgI seeding in prior idealized studies, LP is weaker in both magnitude and spatial extent because LP-generated ice requires a continuous SLW cloud layer for dispersion from the surface to clouds. Nevertheless, LP is effective at temperatures warmer than -6 °C where AgI is less active, suggesting complementary roles of the two seeding agents. These simulations provide a physical basis for understanding LP seeding responses and for future three-dimensional real-case simulations, field evaluation, and direct comparison with AgI seeding simulations.

1. Introduction

Winter orographic storms over western North America frequently produce supercooled liquid water (SLW) in shallow cloud layers above the windward slope and ridgetop, where condensate supply by terrain-forced ascent can outpace depletion by ice growth (Politovich and Vali 1983; Rauber and Grant 1986). Over coastal and lower-elevation barriers such as the Sierra Nevada, Cascades, and lower Wasatch, SLW occurs most frequently at cloud temperatures between 0 and approximately -10 °C (Heggli and Rauber 1988; Tessendorf et al. 2019; Rauber et al. 2019); SLW is also observed at colder temperatures over higher interior ranges, but with lower frequency and lower water content (Politovich and Vali 1983; Rauber et al. 2019). Conventional silver iodide (AgI) seeding is relatively inefficient at the warmer end of this range (DeMott 1995; Marcolli et

https://doi.org/10.5194/egusphere-2026-3289
Preprint. Discussion started: 2 July 2026

al. 2016), motivating the search for agents that can efficiently convert SLW to ice in relatively warm environments. Liquid propane (LP) meets these requirements because rapid expansion and vaporization of the liquid cause intense local cooling, producing extremely high ice crystal yields in slightly supercooled clouds. Early California and Utah design studies therefore centered on propane as a means of increasing snowpack over target basins when suitable SLW is present but AgI effectiveness is limited.

The microphysical basis for propane seeding was established in the 1970s and early 1980s through field and laboratory work that quantified its ice-nucleating potential and crystal characteristics. Hicks and Vali (1973; hereafter HV73) demonstrated that liquefied propane sprays can generate very large concentrations of ice crystals in supercooled cloud volumes, with strong temperature dependence and crystal habits consistent with rapid freezing of cloud droplets. Kumai (1982; hereafter K82) used controlled cold-room experiments to quantify the ice-crystal production rate of evaporating LP from -0.1 to -40 °C, reporting yields of approximately 10^{11} ice crystals per gram of propane below about -5 °C and characterizing early-stage crystal habits by electron microscopy. In physical terms, the release of LP as a fine mist causes rapid vaporization and expansion, cooling the air near the nozzle to -40 °C or colder. This extreme local cooling initiates immediate homogeneous ice nucleation (Reynolds, D. W., 1989; Super and Holroyd, 1997; Super and Heimbach 2005). This process is distinct from heterogeneous ice nucleation by AgI, which requires the seeding agent to act as a substrate for ice formation. Because the propane plume locally cools well below the homogeneous freezing temperature, LP can nucleate ice at any cloud temperature below 0 °C, whereas operational AgI requires temperatures colder than approximately -6 to -8 °C to produce significant ice concentrations (DeMott 1995; Marcolli et al. 2016). LP is therefore well suited to slightly supercooled, SLW-rich clouds in environments warmer than the AgI activation threshold.

Building on these microphysical results, Reynolds et al. (1989, 1991, 1994) designed ground-based LP snowpack augmentation programs in the Sierra Nevada, and the Utah program subsequently refined this approach by developing automated dispensers on the Wasatch Plateau during the 1990s (Super et al. 1995; Super 1999, Super and Heimbach 2005; Holroyd and Super 1998). Super et al. (1995) described dispenser testing during the winters of 1992-93 and 1993-94, including calibration of release rates, assessment of mechanical reliability, and a prototype system that used telemetered SLW, wind, and temperature measurements to control multiple sites automatically. Subsequent experiments integrated propane with AgI in coordinated physical seeding studies that used aircraft and ground-based microphysics to evaluate in-cloud responses. Both programs demonstrated that propane could be handled and released operationally across multiple sites along mountain crests. Super and Holroyd (1997) reported physical evidence of LP seeding effects in slightly supercooled orographic clouds, documenting localized increases in ice particle number and changes in crystal habit when seeded plumes intersected SLW-rich regions. These results reinforced the operational conclusion that propane release must be restricted to periods when the generator is embedded in cloud, and that propane is particularly valuable for warmer, SLW-rich storms where AgI is less effective.

Later analyses of California LP seeding operations used sulfur hexafluoride (SF6) as a passive tracer to track plume transport and dispersion, showing that seeded plumes were strongly modulated by gravity waves and terrain flows (Reynolds 1996).

https://doi.org/10.5194/egusphere-2026-3289
Preprint. Discussion started: 2 July 2026

Clear seeding signatures were detected in only a subset of plume intersections, largely because many plumes traversed regions with little or no SLW, underscoring the critical dependence of LP seeding efficacy on the microphysical environment. Across these programs, LP is portrayed as a powerful but conditional seeding agent whose success depends on accurate SLW diagnosis, careful siting of in-cloud generators, and improved modeling tools to link plume evolution to precipitation outcomes.

Despite this long history and the operational maturity of LP dispensing systems, recent activity has been relatively sparse compared with AgI. A recent structured dataset of U.S. cloud-seeding activities (Donohue and Lamb, 2025) confirms that AgI remains the dominant seeding agent, with very few programs using LP over the past two decades. Activity has picked up again in recent years, however, as interest has grown in enhancing winter precipitation in warmer climates. Idaho Power has been developing and testing LP generators for several years and began operational LP seeding alongside AgI in the Payette Basin in winter 2023-24 during the Idaho Liquid Propane Experiment (LPX) Phase I (Dawson et al. 2026).

Despite these renewed field efforts, liquid propane remains only sparsely represented in the modeling literature. There are essentially no numerical studies that explicitly treat LP seeding with a physically based parameterization. This lack of model representation limits our ability to investigate the microphysical pathways, plume-cloud interactions, and precipitation responses associated with LP seeding, and it hinders quantitative evaluation of its potential under different environmental conditions. A physically based LP modeling capability would allow quantitative evaluation of LP seeding under controlled conditions, complementing existing AgI simulation capability and supporting operational decisions in programs that increasingly deploy LP. Numerical modeling studies of AgI seeding have been far more extensive, including idealized and real-case simulations that trace the chain from ice nucleation to precipitation enhancement (e.g., Xue et al. 2013a,b, 2022; Chen et al. 2023, 2025; Harrold et al. 2026). These studies have demonstrated the value of process-based modeling for understanding seeding mechanisms and guiding operational decisions.

This study addresses the LP modeling gap by developing and implementing a temperature-dependent liquid propane ice nucleation parameterization within the Weather Research and Forecasting (WRF) model, enabling explicit simulation of LP-induced ice production and its impacts on cloud microphysics and precipitation. Two empirical formulations, based on the laboratory data of HV73 and K82, are implemented within the Thompson microphysics scheme. The parameterization is evaluated through a systematic series of idealized two-dimensional simulations designed to isolate the sensitivity of LP seeding impacts to mountain height, environmental sounding, nucleation formulation, and LP release rate.

The specific objectives are: (1) develop and implement physically based LP ice nucleation formulations within WRF, providing a new numerical modeling capability for LP seeding studies; (2) characterize the physical mechanism by which LP seeding modifies cloud microphysics and precipitation in idealized orographic settings; (3) quantify the sensitivity of LP seeding impacts to environmental conditions, nucleation formulation, and release rate; and (4) establish a foundation for future three-dimensional studies and field experiment comparisons. This paper focuses on idealized two-dimensional simulations as a controlled process study, and model-observation comparison is deferred to future investigations.

https://doi.org/10.5194/egusphere-2026-3289
Preprint. Discussion started: 2 July 2026

2. Model Configuration, Parameterization, and Experimental Design

2.1 Model configuration

In this study, WRF version v4.2.2 (Skamarock et al. 2008) is used in an idealized two-dimensional configuration adapted from Xue et al. (2013a), with small modifications to mountain geometry, grid resolution, sounding profiles, and vertical coordinates. The model domain spans 800 km in the x direction (400 grid points at 2 km spacing) with 61 vertical levels on a hybrid eta coordinate and a model top at 23 km. The time step is 6 s, all simulations are integrated for 20 hr, and output is saved every 15 min.

The Thompson aerosol-aware microphysics scheme (Thompson and Eidhammer 2014) provides prognostic treatment of cloud water, rain, cloud ice, snow, and graupel mixing ratios, as well as cloud-ice and rain number concentrations. Radiation, surface-layer, planetary boundary-layer, and cumulus parameterizations are turned off so that the seeded response can be interpreted in a controlled idealized framework. Rayleigh damping is applied above 10 km, lateral boundaries are open in x and periodic in y, and the model uses nonhydrostatic dynamics with sixth-order numerical diffusion.

The terrain is a bell-shaped mountain defined by

$$h(x) = (h0/16)\,[1 + \cos(\pi\,(x - x0)/(4\,a0))]^4, \text{ for } |x - x0| < 4\,a0,$$

$$h(x) = 0 \text{ otherwise.}$$

Here h0 is the peak mountain height and a0 is the half-width parameter. Both terrain configurations considered here use a0 = 50 km. The two terrain heights are investigated h0 = 1000 m (referred to as HM1000m) and 1500 m (referred to as HM1500m). Figure 1 shows the mountain geometries, the surface generator location, and the downstream analysis region. The two terrain groups therefore differ only in mountain height, allowing the response to LP seeding to be compared across different degrees of orographic forcing.

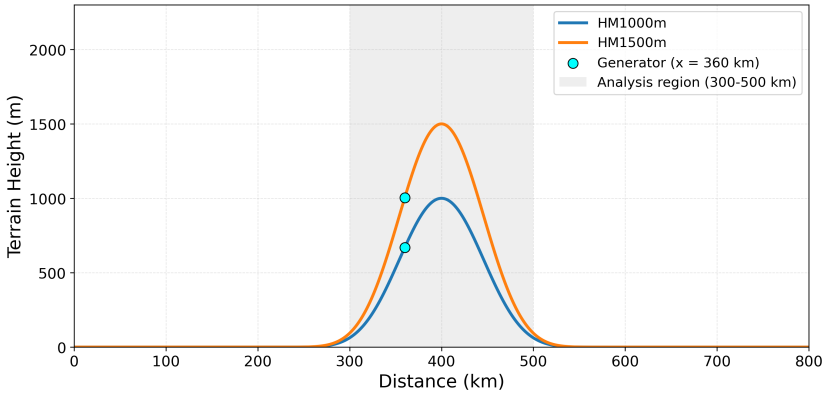

Figure 1. Idealized mountain geometries used in this study. Curves show the HM1000m and HM1500m terrain profiles, cyan circles mark the LP generator location at x = 360 km, and gray shading indicates the downstream analysis region (x = 300-500 km) used for the integrated precipitation diagnostics.

https://doi.org/10.5194/egusphere-2026-3289
Preprint. Discussion started: 2 July 2026

2.2 LP ice nucleation parameterization

Unlike glaciogenic seeding by silver iodide, LP seeding does not act through an ice-nucleating particle. Instead, rapid expansion and vaporization of the released LP plume produce intense cooling immediately surrounding the nozzle and freeze droplets in a very small volume near the nozzle. That effective cooling radius of the LP plume (22 inches, Vardiman et al. 1971) is far smaller than the 2-km grid spacing used here, so the unresolved thermodynamic perturbation cannot be meaningfully applied over an entire model grid cell. The resolved quantity of interest is therefore the rate at which LP release produces new ice crystals in cloudy, subfreezing air.

Two empirical LP ice-production formulations were implemented based on the laboratory studies by Hicks and Vali (1973; HV73) and Kumai (1982; K82). The fitted relations and the underlying laboratory data are shown in Figure 2. The coefficients were derived by the present authors by fitting the exponential form to ice-production rates digitized from the published scatter plots. The parameterization uses

$$Ni(T) = a \exp[b/(T - 273.15)],$$

where Ni is the number of ice crystals produced per second per kilogram of LP released and T is air temperature in kelvin. The fitted coefficients are a = 4.33 x 10^{14} and b = 1.25 for HV73, and a = 1.60 x 10^{14} and b = 5.41 for K82. HV73 yields more ice (approximately 3-6 times of K82 ice production for temperature <-5 °C, Figure 2b) and has the steeper temperature dependence near the freezing point. Together, the two fits provide a practical range for examining formulation sensitivity.

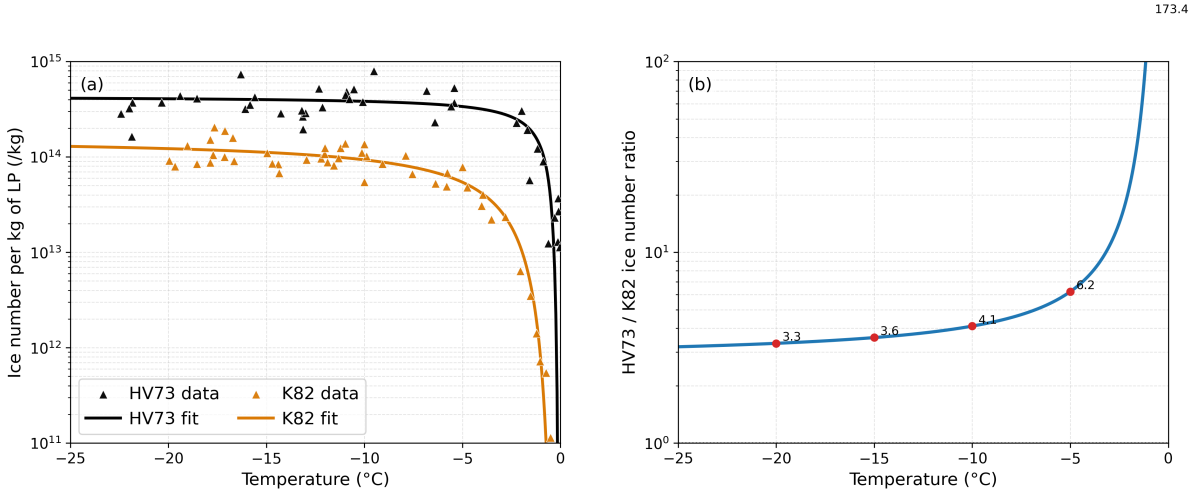

Figure 2. (a) Laboratory ice-crystal production as a function of temperature from Hicks and Vali (1973; HV73) and Kumai (1982; K82). Symbols denote data points from the laboratory measurements, and lines show the fitted relationships used in the LP parameterization. (b) Ratio of ice production between fitted HV73 and K82 curves as a function of temperature.

https://doi.org/10.5194/egusphere-2026-3289
Preprint. Discussion started: 2 July 2026

2.3 Experimental design

The experimental design is intended to examine sensitivity to terrain forcing, environmental conditions, nucleation formulation, and release rate. It comprises two mountain heights, four environmental soundings, and five scenarios for each mountain-sounding combination: one control run and four seeded runs.

The initial atmospheric profiles are constructed analytically following the framework used in earlier idealized orographic seeding studies by Xue et al. (2013a). Figure 3 compares the sounding profiles used in this study, and Table 1 summarizes the set of simulations analyzed here. The Default sounding has a sea-level temperature of 273.15 K (0 °C), a dry Brunt-Vaisala frequency of 0.011 s^{-1}, a low-level relative-humidity parameter of 0.90 with a 1500-m decay scale, surface pressure of 1000 hPa, and a uniform 10 m s^{-1} wind in the x direction. This profile yields a true surface relative humidity of about 81.7 % and a surface water-vapor mixing ratio of 3.11 g kg^{-1}.

Table 1. Summary of the simulations conducted in this paper. Two terrain heights, four environmental soundings, and five seeding scenarios are considered, resulting in 40 simulations in total.

Terrain group	Mountain height (m)	Environmental soundings	Seeding scenarios
HM1000m	1000	Default, Cold, Dry, Warm	CTRL, LP1xHV73, LP2xHV73, LP1xK82, LP2xK82
HM1500m	1500	Default, Cold, Dry, Warm	CTRL, LP1xHV73, LP2xHV73, LP1xK82, LP2xK82
Total		2 terrain groups x 4 soundings	5 scenarios per terrain-sounding combination

https://doi.org/10.5194/egusphere-2026-3289
Preprint. Discussion started: 2 July 2026

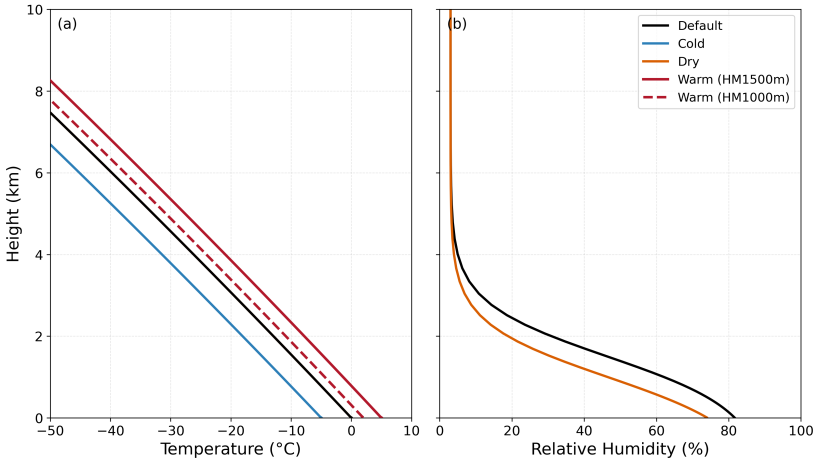

Figure 3. Initial sounding profiles used in this study. Panel (a) shows temperature for the Default, Cold, Dry, Warm (HM1500m), and Warm (HM1000m) soundings. Panel (b) shows relative humidity for the Default and Dry soundings; the Cold and Warm soundings use the same relative-humidity profile as Default.

Three sounding perturbations are applied relative to this reference profile. The Cold sounding lowers the sea-level temperature by 5 K, yielding a colder and drier profile with a surface water-vapor mixing ratio of 2.14 g kg^{-1}. The Dry sounding retains the Default temperature but reduces the humidity decay scale from 1500 to 1000 m, producing drier conditions aloft and a surface water-vapor mixing ratio of 2.94 g kg^{-1}. The Warm sounding increases the sea-level temperature by 5 K for HM1500m, raising the surface water-vapor mixing ratio to 4.44 g kg^{-1}. For HM1000m, the warm perturbation is reduced to 2 K (275.15 K, 3.59 g kg^{-1}) so that the seeded cloud layer remains supercooled and LP seeding remains physically relevant.

For each mountain-sounding combination, five simulations are performed: one control (CTRL) and four seeded runs using K82 and HV73 at two LP release rates. The baseline LP release rate is 3.66 x 10^{-3} kg s^{-1} (LP1x, equivalent to 6 gallons hr^{-1}), and the doubled release rate is 7.32 x 10^{-3} kg s^{-1} (LP2x, 12 gallons hr^{-1}). The total LP mass released during the 300-min seeding window is 65.9 kg for LP1x and 131.8 kg for LP2x. The generator is located at the surface on the windward slope (x = 360 km) and is embedded within the supercooled cloud layer during the seeding period in all 8 environments considered here. The paper therefore analyzes 2 x 4 x 5 = 40 simulations.

In the model, LP is released from a prescribed surface generator on the windward slope, 40 km upwind of the mountain peak. The seeding window spans between 450 min and 750 min. The LP mass release rate (kg s^{-1}) is converted to a volumetric source term by dividing by the local grid-cell volume. Multiplying that source term by Ni(T) gives a cloud-ice number tendency (m^{-3} s^{-1}). A corresponding cloud-ice mass tendency is obtained by assigning each newly generated crystal an initial mass of 1 x 10^{-12} kg, consistent with the Thompson cloud-ice category. The LP source is applied only in cloudy, subfreezing cells where cloud water is present, so ice is produced only in the intended mixed-phase environment and the singular behavior of the temperature relation at 0 °C is avoided. The resulting number and mass tendencies are applied to the

https://doi.org/10.5194/egusphere-2026-3289
Preprint. Discussion started: 2 July 2026

Thompson cloud-ice prognostic variables at each microphysics call. Once formed, LP-generated ice follows the same deposition, riming, aggregation, sedimentation, advection, and mixing pathways as other model cloud ice.

Unless otherwise noted, precipitation response is evaluated at 14 hr, which is 90 min after the end of seeding. Mean accumulated precipitation is averaged over x = 300-500 km. Both precipitation volume and mean accumulated precipitation are tracked, but precipitation volume is used as the primary magnitude metric in the main text because it better conveys the absolute size of the response across environments with very different control baselines.

3. Results

3.1 Natural cloud and precipitation characteristics across environments

Figure 4 shows the control cross-sections at t = 750 min for HM1000m and HM1500m. The control clouds differ systematically across both sounding and terrain height. HM1500m supports deeper clouds and stronger natural precipitation development than HM1000m, consistent with stronger orographic lift. Within each terrain group, the Cold and Default soundings sustain broader mixed-phase cloud regions than Warm, while Dry suppresses condensate aloft and narrows the cloud. The HM1500m Warm case also shows the strongest natural rain development of the eight environments considered here. Overall, the natural precipitation varies more than one order of magnitude across the simulations, from less than 0.01mm in HM1000m Dry to 0.25 mm in HM1500m Cold (Table 2). These differences in natural conditions provide the background for interpreting why the seeded response varies so strongly across the set of simulations.

https://doi.org/10.5194/egusphere-2026-3289
Preprint. Discussion started: 2 July 2026

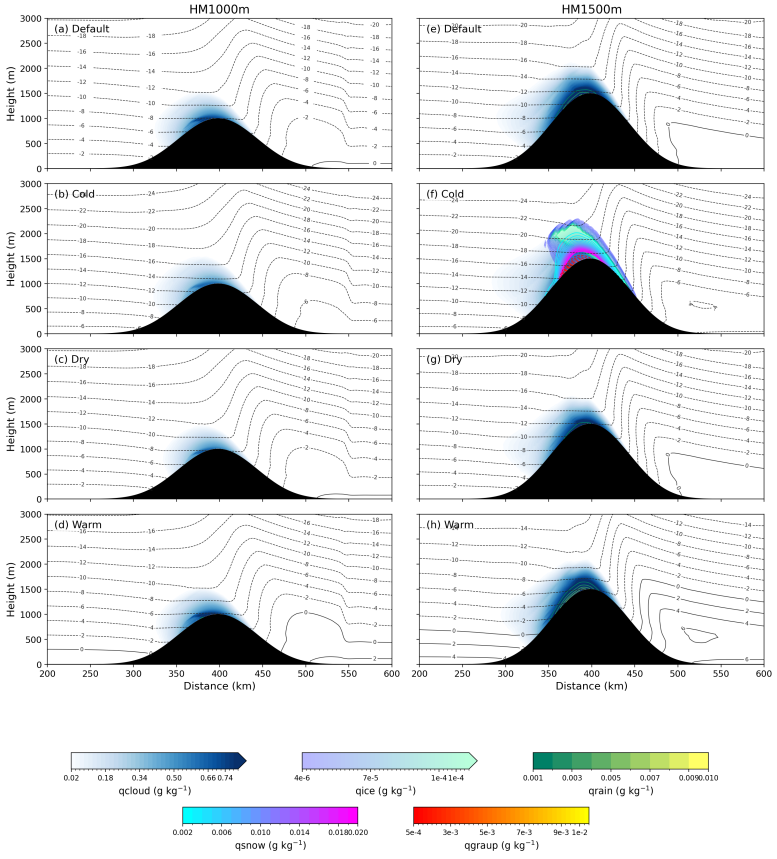

Figure 4. Cloud cross-sections at t = 750 min for the HM1000m and HM1500m environments in Control. Rows show the Default, Cold, Dry, and Warm soundings; columns compare HM1000m and HM1500m. Blue shading shows qcloud, the translucent winter shading shows qice, green contours show qrain, cyan contours show qsnow, orange dashed contours show qgraup, and gray contours show temperature at 2 °C intervals.

3.2 Seeding impacts on accumulated precipitation

LP seeding produces positive precipitation responses across the majority of simulated environments (Figure 5; Table 2). All 16 HM1000m simulations show precipitation increases, and 12 of the 16 HM1500m simulations also respond positively, though with a smaller magnitude in precipitation enhancement. All relative responses larger than 10 % occur in HM1000m, where the natural precipitation is lower as a result of weaker orographic forcing and lower absolute precipitation enhancement. This implies the cloud microphysical environment may be more amenable to LP-induced modification in a shallow mountain slope. HM1500m responses are weaker overall, with Cold, Dry, and Default remaining modestly positive and Warm producing weakly negative cases, all small in magnitude (smaller than 7.3 x 10^2 m^3 or 0.3 %).

Cold and Dry in HM1000m produce nearly equal relative seeding impacts (Figure 5b), but Cold produces more absolute gain in volume (Figure 5a). This is because Cold produce more natural precipitation, but at the same time more ice per unit LP released is generated as a result of a colder environment at the seeding site. In contrast, Dry and Default produce similar

https://doi.org/10.5194/egusphere-2026-3289
Preprint. Discussion started: 2 July 2026

absolute impact, but due to the more efficient natural precipitation in Default, relative impact in Dry is four times as large as Default. Therefore, traditional statistical metrics of cloud seeding impacts using relative enhancement in % should be viewed together with an absolute amount to get a better context understanding of the actual seeding impacts.

Warm produces the weakest seeding response in both absolute and relative terms. Warm remains supercooled at the seeding site, but the seeded cloud layer is warmer. LP ice production is reduced, and the background cloud is already more efficient at producing precipitation. Taken together, these cases show that LP response is most sensitive to environmental conditions that maintain SLW near the release site while limiting the efficiency of the unseeded precipitation response.

In HM1500m, the Cold, Dry, and Default soundings remain positive, but their mean relative responses are only 0.82 %, 2.40 %, and 0.64 %, respectively (Table 2). The HM1500m Warm case is weakly negative under all four seeded scenarios, with a mean relative response of -0.22 %.

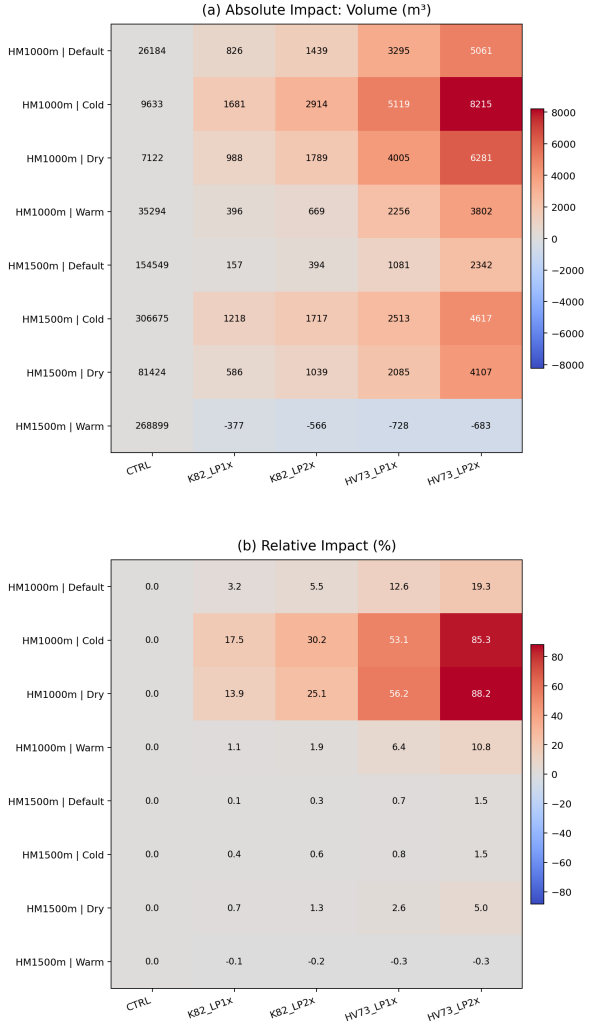

https://doi.org/10.5194/egusphere-2026-3289
Preprint. Discussion started: 2 July 2026

Figure 5. Precipitation response at 14 hr across the 40 simulations analyzed in this study for x = 300-500 km. Panel (a) shows the seeded-minus-control precipitation-volume change (m^3), and panel (b) shows the corresponding relative precipitation impact (%) for each terrain-sounding environment and seeding scenario. In panel (a), the CTRL column annotations give the absolute control precipitation volume for comparison, while the cell colors still denote seeded-minus-control response.

Table 2. Average accumulated precipitation in Control (no seed) and changes due to LP seeding over x = 300-500 km at 14 hr. Mean absolute impact (mm) and Mean relative impact (%) are averages across the four seeded scenarios (LP1xK82, LP2xK82, LP1xHV73, LP2xHV73). LP-mass-normalized efficiency is defined as precipitation-volume change per kilogram of released LP.

Mountain	Sounding	Control (mm)	Mean absolute impact (mm)	Mean relative impact (%)	K82 1x efficiency (m^3 kg^{-1})	K82 2x efficiency (m^3 kg^{-1})	HV73 1x efficiency (m^3 kg^{-1})	HV73 2x efficiency (m^3 kg^{-1})
HM1000m	Cold	0.0079	0.0037	46.53	25.5	22.1	77.7	62.3
HM1000m	Dry	0.0059	0.0027	45.85	15.0	13.6	60.8	47.7
HM1000m	Default	0.0216	0.0022	10.14	12.5	10.9	50.0	38.4
HM1000m	Warm	0.0291	0.0015	5.05	6.0	5.1	34.2	28.9
HM1500m	Dry	0.0672	0.0016	2.40	8.9	7.9	31.7	31.2
HM1500m	Cold	0.2530	0.0021	0.82	18.5	13.0	38.1	35.0
HM1500m	Default	0.1275	0.0008	0.64	2.4	3.0	16.4	17.8
HM1500m	Warm	0.2219	-0.0005	-0.22	-5.7	-4.3	-11.0	-5.2

3.3 Precipitation distribution and phase partition

In all four environments in HM1000m, seeding changes the precipitation partitioning along the windward slope and downstream region rather than producing a spatially uniform increase. Figure 6 shows the accumulated precipitation distributions along the mountain at 14 hr for HM1000m in the control and in the corresponding seeded case LP2xHV73 as an example. The largest total enhancement occurs in Cold and Dry, where the natural precipitation process is relatively weak and dominated by rain. In contrast, Default and especially Warm, marked with slightly more efficient rain process, show weaker precipitation enhancement. The most prominent precipitation enhancement appears near the seeding site, with a prominent snow enhancement, contributing to a major total precipitation peak ahead of the natural precipitation peak (Figure 6). For comparison, Figure 7 shows the corresponding HM1500m accumulated precipitation distributions at the same evaluation time. HM1500m has a much stronger natural precipitation, particularly in Warm, and much smaller seeding impacts relative to control. This generates a secondary peak ahead of the natural precipitation peak (Figure 7).

https://doi.org/10.5194/egusphere-2026-3289
Preprint. Discussion started: 2 July 2026

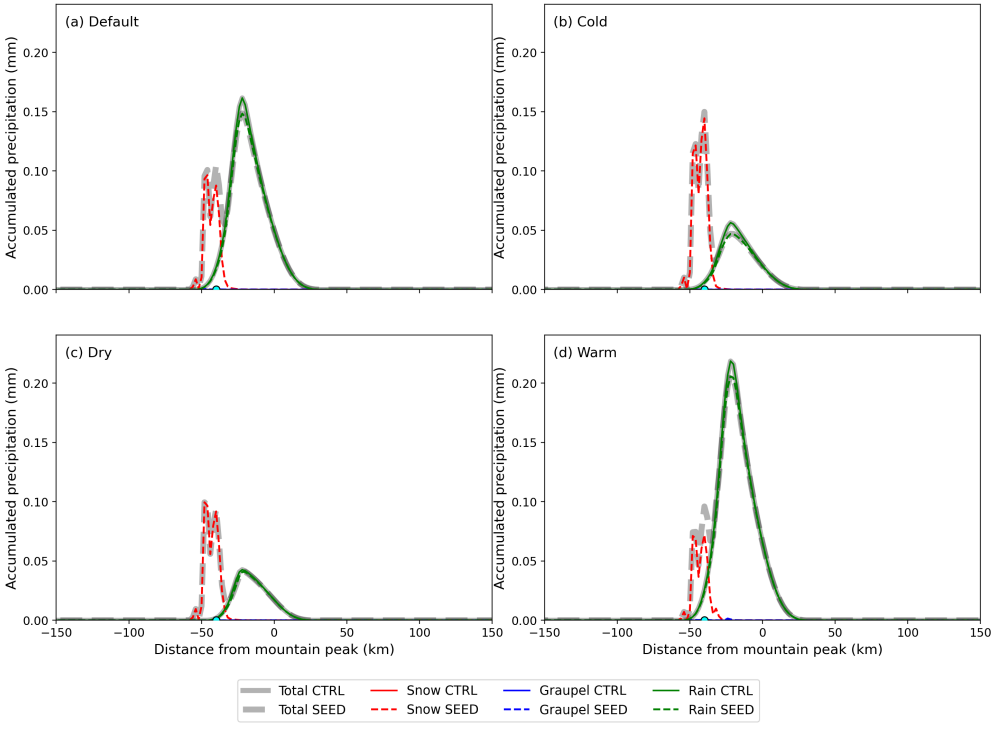

Figure 6. Accumulated precipitation distributions at t = 14 hr for HM1000m in seeded case LP2xHV73. Solid colored lines show the CTRL snow, graupel, and rain components, dashed colored lines show the corresponding seeded components, the solid light-gray line shows Total CTRL, and the dashed light-gray line shows Total SEED. Panels compare the (a) Default, (b) Cold, (c) Dry, and (d) Warm soundings.

https://doi.org/10.5194/egusphere-2026-3289
Preprint. Discussion started: 2 July 2026

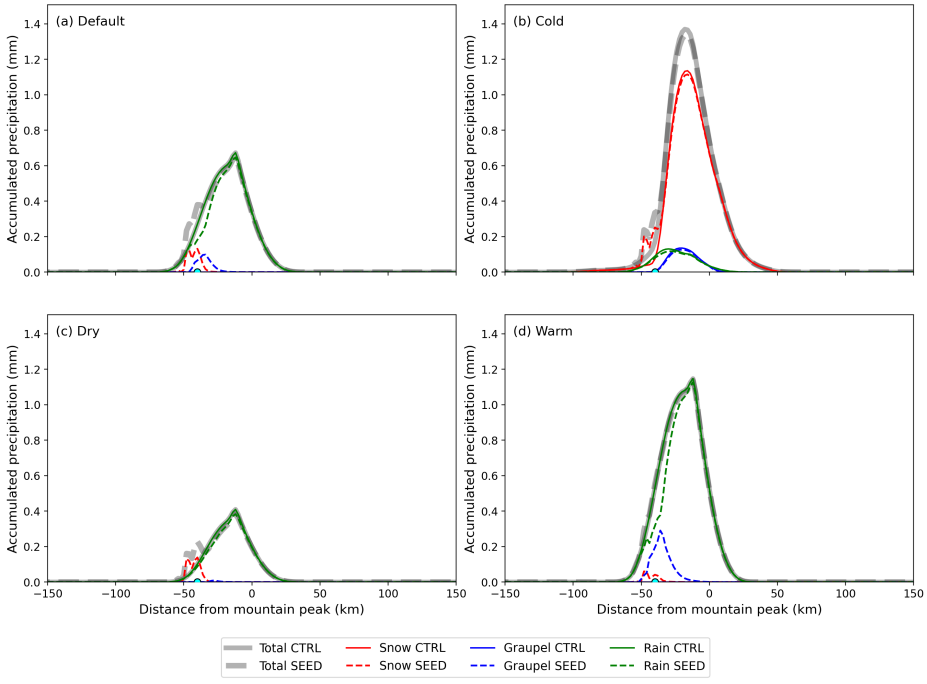

Figure 7. Same as Figure6 but for HM1500m.

The seeded-minus-control distributions in Figure 8 and Figure 9 further reveal that the seeding impacts on precipitation type and phase depends on the mountain geometry and the atmospheric profile. In HM1000m environments, where the natural rain process is very weak at the seeding site, LP-induced ice primarily converts supercooled liquid cloud water to snow near the seeding location (approximately between -60 to -20 km distance from the mountain peak, Figure 8). Graupel production through riming is negligible because few raindrops are available for collection. The dominant seeding response in these environments is therefore snow enhancement near the seeding location with a modest downstream rain reduction due to SLW depletion by the additional ice. The snow enhancement location does not shift with cases, only magnitude changes (Figure 8).

https://doi.org/10.5194/egusphere-2026-3289
Preprint. Discussion started: 2 July 2026

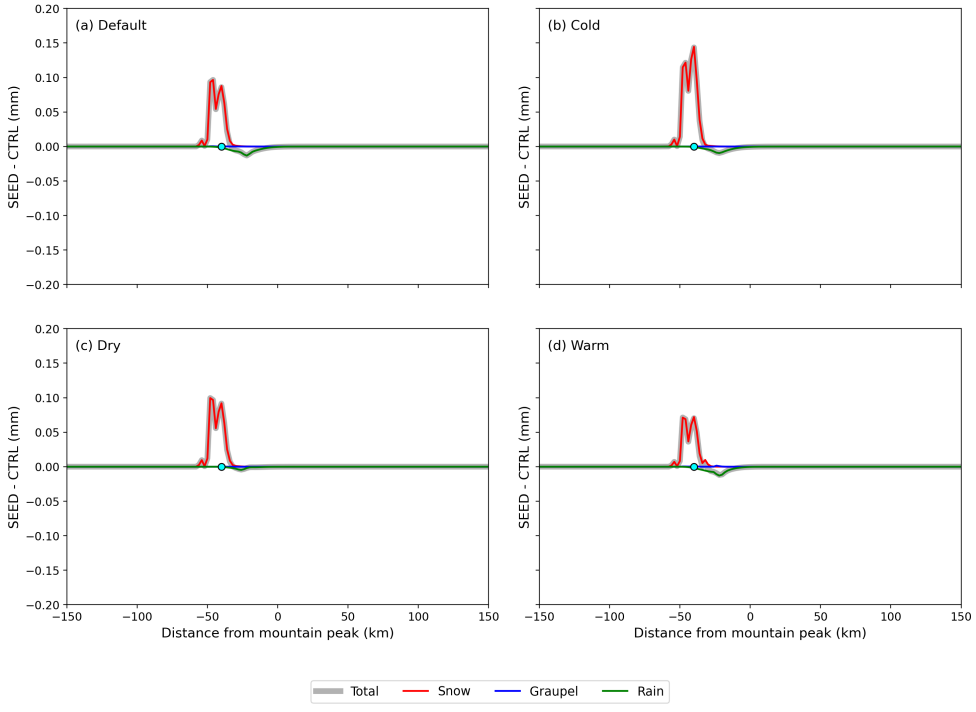

Figure 8. Seeded-minus-control precipitation distributions at t = 14 hr for HM1000m in LP2xHV73. Colors distinguish snow, graupel, rain, and total precipitation. Panels compare the (a) Default, (b) Cold, (c) Dry, and (d) Warm soundings.

In HM1500m environments, the dominant positive contribution to total precipitation also comes from increased snow, and the snow enhancement region appears in the similar location as in HM1000m (Figure 9). The general spatial pattern of seeding impacts in these high mountain experiments is prominent precipitation enhancement near the seeding location (approximately -60 km to -35 km distance from the mountain peak) and a mild reduction in the immediate downwind (approximately -35 km to 10 km). However, detailed microphysical causes to the precipitation changes differ in these cases. This is because HM1500m environments produce more diverse natural clouds and precipitation profiles than in the HM1000m (Figure 4 and Figure 8). Natural rain development is generally more active at the seeding location in HM1500m, in particular in Default and Warm (Figure 7 and 8), efficient graupel enhancement through riming appears near the seeding site as well as further downwind of the snow enhancement region, which co-located with the region where strong rain reduction occurs (Figure 9), reflecting strong conversion of raindrops to graupel. However, the peak of graupel formation appears upstream of the peak of precipitation, because the ice generated from the seeding location starts to fall out quickly as soon as graupel forms while natural precipitation keeps developing further upslope. It is also shown that the graupel enhancement in the rain dominant region could inhibit rain reduction than the graupel enhancement, leading to a small precipitation reduction. In Default, the strong snow enhancement offset the reduction near the seeding site, producing an overall marginal precipitation enhancement. In Warm where (unrimed) snow enhancement is weak, leading to a marginally precipitation reduction. Due to snow falls in the upstream of graupel and rain, there is also a spatial difference in

https://doi.org/10.5194/egusphere-2026-3289
Preprint. Discussion started: 2 July 2026

precipitation changes dominated by snow enhancement near the seeding location (approximately -60 km to -35 km distance from the mountain peak) and rain reduction at the downwind (-40 km to 10 km). Unlike the other three cases, natural precipitation in Cold is predominant by mixed-phase processes with snow as the main precipitation type (Figure 7b and Figure 4f). Seeding in the naturally mixed-phase clouds generates the highest snow enhancement of all cases (Figure 9b). However, it also suppresses the already active ice precipitation (snow and graupel) in the downwind, producing a mild downwind reduction.

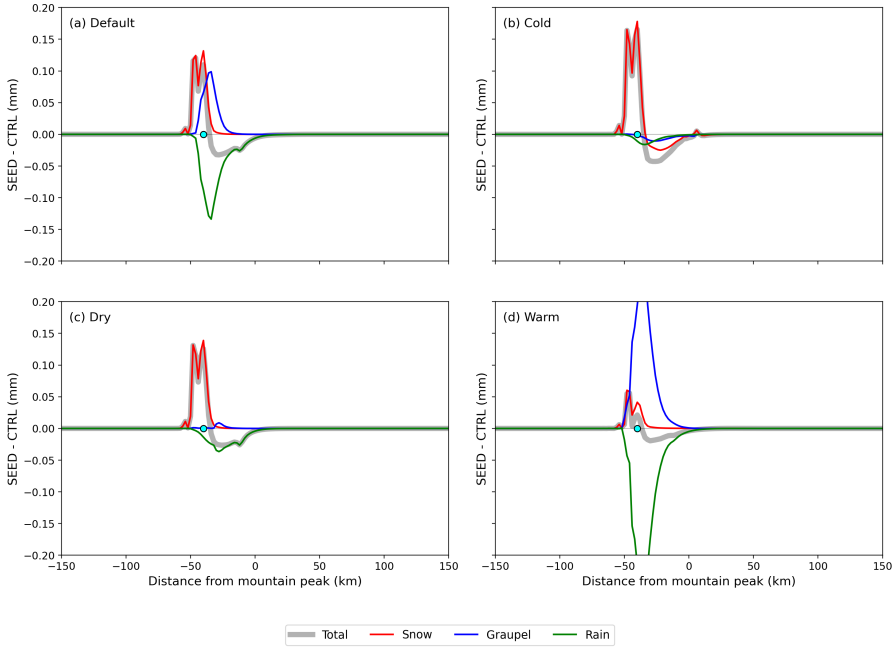

Figure 9. Same as Figure 8 but for HM1500m.

The time series accumulated precipitation shows the immediate snow enhancement during the seeding operation (gray shade in Figure 10) and plateau or reduction right after seeding operation ends, showing that the snow growth through deposition and aggregation happens has a fast response timescale and falls out quickly. In contrast, rain and graupel changes happen downstream and lags in time, with its trend starting and reaching a plateau slightly later than snow. Snow is the dominant positive response in most cases, growing steadily after seeding begins, while rain and graupel changes remain comparatively small, consistent with limited riming in this weak-rain environment. This general pattern contrasts with HM1500m Warm, where graupel increases sharply at the expense of rain and snow enhancement remains weak, reflecting active riming in an efficient-rain environment.

https://doi.org/10.5194/egusphere-2026-3289
Preprint. Discussion started: 2 July 2026

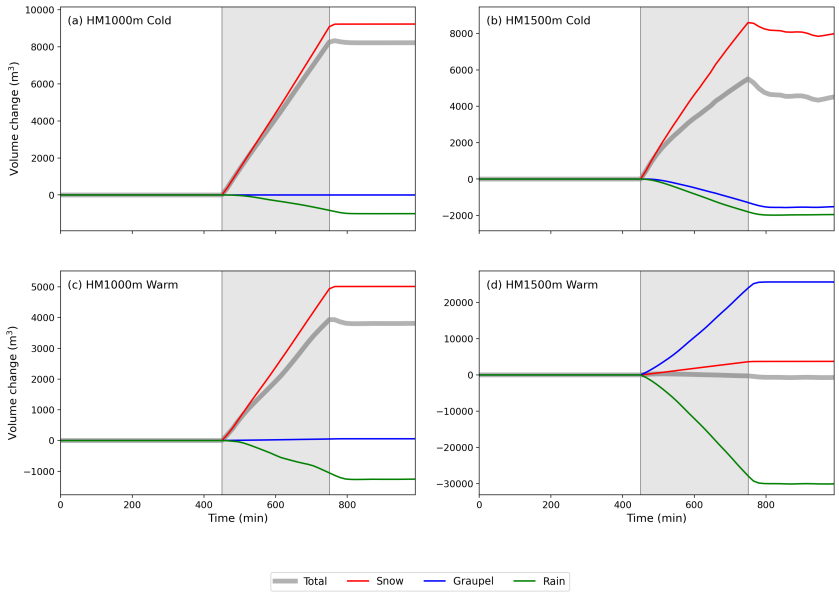

Figure 10. Time series of accumulated precipitation-volume changes (m^3) over x = 300-500 km between SEED (LP2xHV73) and CTRL (no seed) for the Cold case (top) and Warm (bottom) in HM1000m (left) and HM1500m (right). Colors distinguish snow, graupel, rain, and total precipitation. Gray shading marks the seeding operational period.

The HM1500m Warm negative response, though small, is consistent across all four seeded scenarios and therefore reflects a systematic redistribution of precipitation in space and time rather than a numerical artifact. In this warm, efficient-rain environment, the natural cloud already converts moisture to rain effectively, leaving less opportunity for LP-induced ice to generate additional precipitation. This contrasts with the positive HM1000m cases, where ice conversion near the seeding site is followed by snow enhancement that more than compensates for any local rain reduction.

3.4 Dependence on nucleation formulation and LP release rate

For cases with positive seeding effects, sensitivity to LP release rate shows that doubling the release rate on average will increase the total precipitation enhancement by half (Table 2). Switching from K82 to HV73 on average yield 3-6 times of total precipitation enhancement, which agrees with the range of ice production enhancement between K82 and HV73 for temperature colder than -5 °C. In HM1500m Warm where marginally precipitation reduction is observed, the scaling rule does not hold.

Figure 11 shows the precipitation enhancement sensitivity to LP release rate for Cold and Warm in both mountain heights. The precipitation enhancement increases monotonically when switching to a higher release rate or a more active ice generating scheme, and the ratio of enhancement between the seeding scenarios remain almost constant throughout the simulation (Figure 11 second column). For Cold in both HM1000m and HM1500m, the enhancement ratios are similar. For HM1000m, the enhancement ratio between HV73 and K82 in Warm is much higher than its corresponding Cold case, which is consistent with the parameterization formula that at a temperature close to freezing, the ice production ratio between

https://doi.org/10.5194/egusphere-2026-3289
Preprint. Discussion started: 2 July 2026

HV73 and K82 is much higher than in a colder temperature regime (<-5 °C). In HM1500m Warm where marginal precipitation reduction at the end of seeding is observed, the trend is nonlinear. The seeding-induced total precipitation mass changes first increase to positive followed by a reduction to negative (Figure 11m), the later stage is contributed by a delayed response in rain and graupel reduction. And the distribution plots show a transition from an overall positive signal near 8 hr (Figure 11o) to a final pattern in which small upwind enhancement is outweighed by broader downwind reduction (Figure 11p).

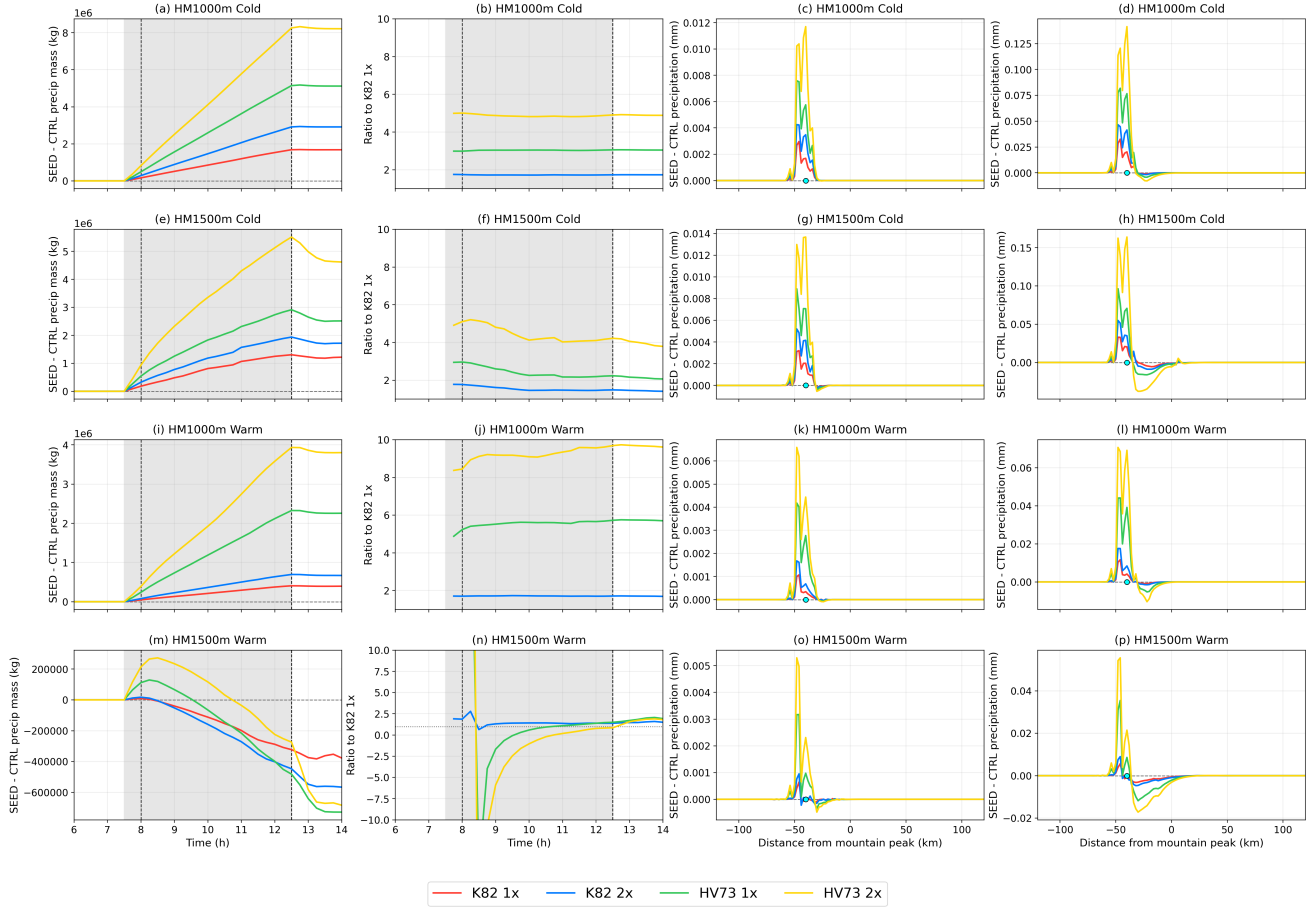

Figure 11. Formulation and release-rate comparison for the Cold and Warm environments. Panels (a)-(d) show HM1000m Cold, panels (e)-(h) show HM1500m Cold, panels (i)-(l) show HM1000m Warm, and panels (m)-(p) show HM1500m Warm. Within each row, the first column shows time series of seeded-minus-control total accumulated precipitation mass on the ground, the second column shows ratio of precipitation enhancement of K82 2x / K82 1x, HV73 1x / K82 1x, and HV73 2x / K82 1x, the third column shows the seeded-minus-control total precipitation distribution at 8 hr (30 min into seeding), and the fourth column shows the seeded-minus-control total precipitation distribution at t = 12.5 hr (at the end of seeding). The 8 hr and 12.5 hr time points are also marked by the two vertical dashed lines in the first and second columns.

Because both HV73 and K82 are derived from limited laboratory datasets, the systematic difference between them also serves as a practical measure of the current uncertainty in the LP ice-production source term. The nonlinear response to doubled release rate in the positive cases, where the mean relative impact increases but LP-mass-normalized efficiency

https://doi.org/10.5194/egusphere-2026-3289
Preprint. Discussion started: 2 July 2026

decreases, is consistent with the environmental constraint: the available SLW and the natural cloud microphysical timescales limit the amount of additional ice that can be converted to precipitation, regardless of LP source strength.

4. Conclusions

This study introduces the first liquid propane ice nucleation parameterization for WRF and evaluates it in idealized two-dimensional simulations under different environments and release rates. The parameterization represents LP release as an ice-production source term tied to LP mass release rate and ambient temperature, implemented within the Thompson aerosol-aware microphysics scheme.

The simulations reveal an environment-dependent cloud microphysical response, in which the ice conversion process near the seeding site (20 km distance from the seeding site) varies with the natural rain efficiency, from a snow-dominated regime where riming is limited to a riming-dominated regime in efficient-rain conditions. Across all positive-response cases, snow enhancement near the seeding location is the dominant contributor to the net surface precipitation increase. Within the low terrain group (1000m), Cold and Dry produce the largest relative responses (~46%), Default is intermediate (~10%), and Warm is weakest (~5%). Seeding responses in the high terrain (1500m) group are weaker overall, with the Warm case producing marginally negative seeding impacts, indicating that LP seeding can redistribute precipitation phases without increasing the total precipitation when the natural rain process is already efficient. The sensitivity to nucleation formulation is also significant: HV73 produces about 3-6 times ice as well as precipitation of the K82 scheme. Because both schemes are derived from laboratory experiments, their difference can serve as a measure of the current uncertainty in the LP ice-production source term.

Compared with AgI seeding as represented in prior idealized studies (e.g., Xue et al. 2013a,b), LP seeding produces weaker impacts in both the magnitude and the spatial extent of precipitation enhancement. AgI seeding materials can be transported to upper levels and further downwind before activating as ice nuclei, whereas LP-generated ice is produced at the LP release source where cooling takes place and requires a continuous SLW cloud layer to sustain its dispersion upward and downwind from the generator. LP seeding is therefore more sensitive to the local environment down to the surface. However, LP is effective at temperatures warmer than -6 °C where AgI activation is limited, so the two agents may serve complementary roles under different atmospheric conditions. Future numerical studies that directly compare AgI and LP seeding within the same model configuration would help quantitatively evaluate their respective seeding impacts and cloud microphysical responses across a range of environments.

Several limitations should be noted when interpreting the present results. The simulations are idealized and two dimensional, so they do not resolve three-dimensional flow structure, turbulence, or complex-terrain-induced variability present in real storms. The current LP parameterization depends only on temperature and release rate and does not yet include explicit dependence on SLW concentration or an environmentally dependent size distribution of LP-generated ice due to limitation in available observational datasets. The experiments use a single microphysics scheme, and no observational comparison is

https://doi.org/10.5194/egusphere-2026-3289
Preprint. Discussion started: 2 July 2026

attempted. In addition, while laboratory studies provide a foundational understanding of LP-induced ice nucleation, they are limited in their ability to capture the full complexity of atmospheric conditions, such as turbulence, cloud structure, and ambient moisture variability, that influence seeding outcomes. Therefore, field observations are essential to validate and refine these parameterizations under real-world conditions, which will provide observational data support with in-situ measurements of ice produced in seeded plumes and further validate or improve our current modeling capabilities. Future evaluation work using three-dimensional real-terrain simulations constrained by observations is important to determine how turbulence and terrain-flow interactions modify the seeded cloud response and to connect the idealized results to current field efforts such as the Idaho Liquid Propane Experiment. The parameterization itself requires further refinement, particularly laboratory measurements that relate LP ice production to both temperature and available liquid water, and characterization of the LP-generated ice size spectrum and its influence on riming, aggregation, and fallout. Taken together, these results demonstrate that LP can be represented in WRF to evaluate seeding response under various environmental conditions, establishing a basis for future more complex simulations, field-oriented evaluation, and comparison with other glaciogenic seeding approaches.

Acknowledgement

This work was funded by the Idaho Department of Water Resources (IDWR) under contract #3645. This material is based upon work supported by the NSF National Center for Atmospheric Research, which is a major facility sponsored by the U.S. National Science Foundation under Cooperative Agreement No. 1852977. High-performance computing support from Derecho (https://doi.org/10.5065/qx9a-pg09) was provided by NSF NCAR's Computational and Information Systems Laboratory (CISL). The authors thank Brandal Glenn from Idaho Power Company for providing the LP release rate data used in this study.

Data availability

The model output data and analysis scripts used to generate the figures in this paper will be deposited in the Zenodo repository, with a DOI assigned, at the time of final publication. Until then, these materials are available upon reasonable request and are accessible to reviewers during the review process.

Author contributions

SC conceptualized the study, developed the LP ice nucleation parameterization and model code, performed the simulations and formal analysis, prepared the figures, and wrote the original draft. LX contributed to the conceptualization and methodology, including the idealized simulation framework. MH contributed to the design and analysis of the numerical

https://doi.org/10.5194/egusphere-2026-3289
Preprint. Discussion started: 2 July 2026

experiments. ST contributed to the conceptualization and provided supervision and funding acquisition. JW contributed to the conceptualization and provided project administration and funding acquisition. DJ and ND contributed to the experiment design. All co-authors contributed to the manuscript preparation and discussions.

Competing interests

The contact author has declared that none of the authors has any conflict of interests.

References

Chen, S., Xue, L., Tessendorf, S., Chubb, T., Peace, A., Ackermann, L., Gevorgyan, A., Huang, Y., Siems, S., Rasmussen, R. and Kenyon, S., 2023. Simulating Wintertime orographic cloud seeding over the snowy mountains of Australia. Journal of Applied Meteorology and Climatology, 62(11), pp.1693-1709.

Chen, S., Xue, L., Tessendorf, S.A., Chubb, T., Peace, A., Kenyon, S., Speirs, J., Wolff, J. and Petzke, B., 2025. Assessing glaciogenic seeding impacts in Australia's Snowy Mountains: an ensemble modeling approach. Atmospheric Chemistry and Physics, 25(13), pp.6703-6724.

Dawson, N., M. Harrold, S.A. Tessendorf, 2026: Pressure-driven Valley Flows in the Snake River Plain: Climatology, Vertical Structure, and Synoptic Context. *Wea. Forecasting*, submitted.

DeMott, P.J., 1995. Quantitative descriptions of ice formation mechanisms of silver iodide-type aerosols. *Atmospheric Research*, *38*(1-4), pp.63-99.

Donohue, J.J. and Lamb, K.D., 2025. Structured dataset of reported cloud seeding activities in the United States (2000–2025) using an LLM. Scientific Data.

Harrold, Michelle, Sarah A. Tessendorf, Lulin Xue, Jamie K. Wolff, Erin Dougherty, Bart Geerts, Alfred R. Rodi, and David Gochis. "Evaluating the Precipitation Impacts of Cloud Seeding in Southern Wyoming and Northern Colorado using WRF-WxMod® within an Ensemble Modeling Framework." Journal of Applied Meteorology and Climatology (2026): e250099.

Hicks, J. R., and G. Vali, 1973: Ice nucleation in clouds by liquefied propane spray. J. Appl. Meteor., 12, 1025-1034.

Holroyd, E. W., III, and A. B. Super, 1998: Experiments with pulsed seeding by AgI and liquid propane in slightly supercooled winter orographic clouds over Utah's Wasatch Plateau. J. Wea. Modif., 30, 52-77.

Heggli, M. F., and R. M. Rauber, 1988: The Characteristics and Evolution of Supercooled Water in Wintertime Storms over the Sierra Nevada: A Summary of Microwave Radiometric Measurements Taken during the Sierra Cooperative Pilot Project. *J. Appl. Meteor. Climatol.*, **27**, 989–1015, https://doi.org/10.1175/1520-0450(1988)027<0989:TCAEOS>2.0.CO;2.

Kumai, M., 1982: Formation of ice crystals and dissipation of supercooled fog by artificial nucleation, and variations of crystal habit at early growth stages. J. Appl. Meteor., 21, 579-587.

https://doi.org/10.5194/egusphere-2026-3289
Preprint. Discussion started: 2 July 2026

Marcolli, C., Nagare, B., Welti, A. and Lohmann, U., 2016. Ice nucleation efficiency of AgI: review and new insights. *Atmospheric Chemistry and Physics*, *16*(14), pp.8915-8937.

Politovich, M. K., and G. Vali, 1983: Observations of Liquid Water in Orographic Clouds over Elk Mountain. *J. Atmos. Sci.*, **40**, 1300–1312, https://doi.org/10.1175/1520-0469(1983)040<1300:OOLWIO>2.0.CO;2.

Rauber, R. M., and Coauthors, 2019: Wintertime Orographic Cloud Seeding—A Review. *J. Appl. Meteor. Climatol.*, **58**, 2117–2140, https://doi.org/10.1175/JAMC-D-18-0341.1.

Rauber, R.M. and Grant, L.O., 1986. The characteristics and distribution of cloud water over the mountains of northern Colorado during wintertime storms. Part II: Spatial distribution and microphysical characteristics. *Journal of climate and applied meteorology*, pp.489-504.

Reynolds, D. W., 1989: Design of a ground-based snowpack enhancement program using liquid propane. J. Wea. Modif., 21, 29-34.

Reynolds, D. W., 1991: Design and field testing of a remote liquid propane dispenser. J. Wea. Modif., 23, 49-53.

Reynolds, D. W., 1994: Further analysis of a snowpack augmentation program using liquid propane. J. Wea. Modif., 26, 12-18.

Reynolds, D.W., 1996. The Effects of Mountain Lee Waves on the Transport of Liquid Propane–Generated Ice Crystals. Journal of Applied Meteorology (1988-2005), pp.1435-1456.

Skamarock, W. C., and Coauthors, 2008: A description of the Advanced Research WRF version 3. NCAR Technical Note NCAR/TN-475+STR, 113 pp.

Super, A.B. and Faatz, E., 1995. A status report on liquid propane dispenser testing in Utah with emphasis on a fully-automated seeding system. The Journal of Weather Modification, 27(1), pp.84-93.

Super, A. B., 1999: Summary of the NOAA/Utah Atmospheric Modification Program: 1990-1998. J. Wea. Modif., 31, 51-75.

Super, A. B., and E. W. Holroyd, 1997: Some physical evidence of AgI and liquid propane seeding effects on Utah's Wasatch Plateau. J. Wea. Modif., 29, 8-32.

Super, A.B. and Heimbach Jr, J.A., 2005. Randomized Propane Seeding Experiment: Wasatch Plateau, Utah. The Journal of Weather Modification, 37(1).

Tessendorf, S. A., and Coauthors, 2019: A Transformational Approach to Winter Orographic Weather Modification Research: The SNOWIE Project. *Bull. Amer. Meteor. Soc.*, **100**, 71–92, https://doi.org/10.1175/BAMS-D-17-0152.1.

Thompson, G. and Eidhammer, T., 2014. A study of aerosol impacts on clouds and precipitation development in a large winter cyclone. Journal of the atmospheric sciences, 71(10), pp.3636-3658.

Vardiman, L., E. D. Figgins, and H. S. Appleman, 1971: Operational Dissipation of Supercooled Fog Using Liquid Propane. *J. Appl. Meteor. Climatol.*, **10**, 515–525, https://doi.org/10.1175/1520-0450(1971)010<0515:ODOSFU>2.0.CO;2.

Xue, L., and Coauthors, 2013a: Implementation of a silver iodide cloud-seeding parameterization in WRF. Part I: Model description and idealized 2D sensitivity tests. J. Appl. Meteor. Climatol., 52, 1433-1457.

https://doi.org/10.5194/egusphere-2026-3289
Preprint. Discussion started: 2 July 2026

Xue, L., and Coauthors, 2013b: Implementation of a silver iodide cloud-seeding parameterization in WRF. Part II: 3D simulations of actual seeding events and the associated effects. J. Appl. Meteor. Climatol., 52, 1458-1476.

455 Xue, L., Weeks, C., Chen, S., Tessendorf, S.A., Rasmussen, R.M., Ikeda, K., Kosovic, B., Behringer, D., French, J.R., Friedrich, K. and Zaremba, T.J., 2022. Comparison between observed and simulated AgI seeding impacts in a well-observed case from the SNOWIE field program. Journal of Applied Meteorology and Climatology, 61(4), pp.345-367.